

PAPER

Differential cross section measurements for ionisation of N₂ in coplanar geometry

To cite this article: Ahmad Sakaamini *et al* 2018 *J. Phys. B: At. Mol. Opt. Phys.* **51** 035207

View the [article online](#) for updates and enhancements.



IOP | ebooks™

Bringing you innovative digital publishing with leading voices to create your essential collection of books in STEM research.

Start exploring the collection - download the first chapter of every title for free.

Differential cross section measurements for ionisation of N₂ in coplanar geometry

Ahmad Sakaamini¹, Matthew Harvey¹, Sadek Amami²,
Andrew James Murray^{1,4} , Don Madison² and Chuangang Ning³

¹Photon Science Institute, School of Physics & Astronomy, University of Manchester, Manchester M13 9PL, United Kingdom

²Missouri University of Science & Technology, Rolla. MO 65409-0640, United States of America

³Department of Physics, State Key Laboratory of Low-Dimensional Quantum Physics, Tsinghua University, Beijing 100084, People's Republic of China

E-mail: Andrew.Murray@manchester.ac.uk and Madison@mst.edu

Received 25 September 2017, revised 29 November 2017

Accepted for publication 1 December 2017

Published 17 January 2018



CrossMark

Abstract

Triple differential cross section measurements for ionisation of N₂ are presented in a coplanar geometry where one of the outgoing electrons was fixed in angle. Data were obtained at incident electron energies 20 and 40 eV above the ionisation potential for the 3σ_g and 1π_u states, the outgoing electrons carrying equal energies. Six sets of measurements were obtained at each energy, with fixed angles of 45°, 90° and 125° to the incident electron direction. The data are compared to new calculations using distorted wave methods.

Keywords: e,2e cross section, DWBA, electron impact ionisation

(Some figures may appear in colour only in the online journal)

1. Introduction

Ionisation of matter by electron impact is a process that occurs throughout the Universe. It is therefore important to provide rigorously tested models of these interactions, so that predictions of the probability of ionisation can be made. These processes occur in stellar and planetary atmospheres [1, 2], in plasmas and in Tokomaks [3], and they play an important role in the interaction of radiation with living cells that may lead to cancer [4]. In these latter cases it is the interaction with low and intermediate energy electrons (typically from threshold to ~100 eV above the ionisation potential (IP)) that has particular relevance, since the probability of DNA damage leading to cell death is highest in this regime.

Quantum mechanical models are essential to describe these interactions at low energies, since both incident electron and target atom (or molecule) must be considered as quantum objects. The models are complicated by the long-range nature of the Coulomb field that governs the forces between the incident electron and the bound electrons and target core. For atomic targets the Coulomb field can be described using a

spherical basis. By contrast, molecular targets do not possess this symmetry, since the nuclei and bound electrons are distributed throughout the molecule. This reduction in symmetry places considerable demands on computation requirements when solving Schrödinger's equation for the interaction. A further complexity arises since the experiments do not generally measure the alignment of molecular targets, and so models must also average over all possible target geometries for a valid comparison to experiment [5].

Additional demands in this energy regime are due to the relatively long time that the electrons interact with the target. Time-dependent models have been used to study these processes for the simplest molecule H₂ [6], however the majority of work on more complex targets (such as N₂ as studied here) adopt time-independent approaches [7–14]. The interaction between the incident electron and target can be modelled using distorted waves [5], and it is also important to include polarisation and correlation effects. Following ionisation the outgoing electrons interact with each other and with the resulting ion, leading to post-collisional interactions (PCI) that can strongly modify the cross section that is measured in the asymptotic region [15]. PCI are particularly important at low energies, and are strongest when the outgoing electrons share the excess energy equally [16].

⁴ Author to whom any correspondence should be addressed.

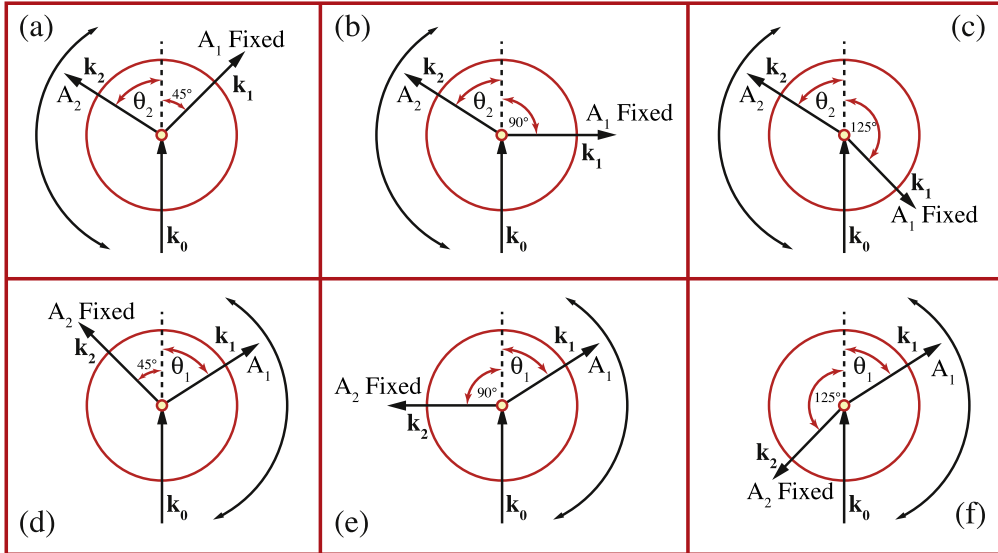


Figure 1. The coplanar geometries in the experiments in section 5. (a) and (d) show the geometry when the fixed angle was 45° , (b) and (e) show where the fixed angle was 90° and (c) and (f) show the geometry for a fixed angle of 125° . The TDCS for both upper and lower configurations must be the same due to reflection symmetry in the scattering plane.

Despite these demands, models of the dynamics of collisional ionisation are becoming increasingly accurate as more is understood about the processes involved. Accurate predictions are now possible for many atomic targets, leading to increased confidence that the essential physics of the interactions are included. The agreement between theory and experiment for molecular targets is however much poorer, and so it is important to provide accurate data for a range of targets to compare to developing models, and to test the different theoretical approaches being formulated.

For single ionisation by electron impact where the spins of the electrons are not detected, the collision can be fully characterised by the incident electron momentum \mathbf{k}_0 and that of the scattered and ejected electrons \mathbf{k}_1 and \mathbf{k}_2 . The most detailed measurements determine a triple differential cross section (TDCS($\mathbf{k}_0, \mathbf{k}_1, \mathbf{k}_2$)) that is proportional to the ionisation probability. The TDCS is experimentally determined by measuring the time-correlated signal between scattered and ejected electrons as a function of $\mathbf{k}_0, \mathbf{k}_1$ and \mathbf{k}_2 in an (e,2e) experiment.

Since the ejected and scattered electrons may emerge from the interaction in any direction, it is necessary to define a scattering geometry to compare theory with experiment. In the work described here in section 5, a coplanar geometry was adopted where the incident, scattered and ejected electrons were detected in the same plane. A further constraint was that one of the electrons was fixed in angle with respect to \mathbf{k}_0 , and the other detected at different angles around the interaction region so as to obtain the relative ionisation probability. The energies of the outgoing electrons were also set equal, so that $|\mathbf{k}_1| = |\mathbf{k}_2|$ and $E_1 = E_2 = (E_{\text{inc}} - \text{IP})/2$.

In practice, the experiment fixed \mathbf{k}_1 and moved \mathbf{k}_2 around the plane, and then fixed \mathbf{k}_2 at the equivalent angle and then moved \mathbf{k}_1 around the plane, as in figure 1. Since the TDCS must be the same for each process, the alignment accuracy of the apparatus could be checked. No difference was found

between measurements under these conditions, and so an average was taken over the series of angular runs that were used. Three different fixed angles were chosen, with $\theta_1(\theta_2)^{\text{Fixed}} = 45^\circ, 90^\circ$ and 125° as depicted.

In a previous set of experiments carried out in Manchester, TDCS data were obtained for ionisation of N_2 in a *doubly-symmetric* geometry, where both electron detectors were set so that $\theta_1 = \theta_2$ and $E_1 = E_2$. These results were compared to calculations from the Missouri group of Don Madison and co-workers [17]. This doubly-symmetric geometry is particularly challenging, since under these conditions the TDCS is highly sensitive to both initial and final states of the system. In the previous work [17] it was found that the models did not predict the data well for the lowest energy studied ($E_1 = E_2 \sim 5$ eV), however as the energy was raised to $E_1 = E_2 = 20$ eV, better agreement was found in the overall shape of the calculated cross sections. It was suggested that further work was needed, including measurements at higher energies to establish if the models improved under these conditions.

The experiments presented in section 4 were hence carried out to ascertain if the models improve at higher energies, and to see how well they predict the TDCS under these conditions. The same energy-sharing conditions (i.e. $E_1 = E_2$) were adopted so that the new data could be directly linked together through their common angles (see below for details). The results using a doubly-symmetric geometry with $E_1 = E_2 = 50$ eV demonstrate that at these energies the predictive-power of the models significantly improves. Following from these experiments, measurements were then taken using the fixed angles as in figure 1, with energies set so that $E_1 = E_2 = 10$ eV and $E_1 = E_2 = 20$ eV.

N_2 is a diatomic molecule whose valence electrons combine to produce a strong triple bond, the electrons pairing to form the $3\sigma_g^2, 1\pi_u^4$ and $2\sigma_g^2$ bonding orbitals and the $2\sigma_u^2$ antibonding orbital. The ground state electronic configuration of N_2

is hence $(2\sigma_g^2 2\sigma_u^2 1\pi_u^4 3\sigma_g^2)^1 \Sigma_g^+$. Ionisation can occur from any orbital, leading to N_2^+ ions in different final states. In the present work ionisation was studied from the two outer orbitals, producing the $X^2\Sigma_g^+ N_2^+$ state for electrons ejected from the $3\sigma_g$ orbital, and the $A^2\Pi_u$ state for electrons emerging from the $1\pi_u$ orbital. The spectrometer could resolve these states, since their binding energies are separated by ~ 1.5 eV, and the average full width at half maximum from fitting Gaussians to these states was ~ 600 meV (see figure 3). Since the final state of the ion is different in each case, the wavefunctions describing the resulting ions is also different, and so this is expected to influence the calculated TDCS.

To discuss these results, this paper is divided into six sections. Following this introduction the experiment is described briefly in section 2. Section 3 summarises the distorted wave models used in the calculations, and section 4 compares experimental and theoretical results for coplanar doubly-symmetric ionisation from the $3\sigma_g$ orbital 100 eV above the IP. Section 5 shows results from measurements at fixed angles for both the $3\sigma_g$ and $1\pi_u$ orbitals, and compares these to calculations. Conclusions are then drawn from these studies in section 6.

2. The experimental apparatus

When set to a coplanar geometry, the (e,2e) spectrometer in Manchester can detect outgoing electrons from the interaction region over a range of angles from $\theta_{1,2} = 35^\circ$ to 125° . These angular restrictions arise due to the size of the electron gun and electron detectors. The electron gun adopts a two-stage electrostatic lens, and can deliver electrons with energy from ~ 20 to 300 eV, with a beam current up to $5 \mu\text{A}$. The scattered and ejected electron analysers use a triple cylindrical lens to focus electrons emerging from the interaction region onto the entrance aperture of a hemispherical energy selector, the selected electrons being detected by a channel electron multiplier. Details of the spectrometer can be found in previous publications (see e.g. [18–20]).

A molecular N_2 beam was delivered from a platinum–iridium gas needle directed into the interaction region. The spectrometer was evacuated to a base pressure of $\sim 10^{-7}$ Torr using a turbo-molecular pump. The vacuum pressure rose to $\sim 2 \times 10^{-5}$ Torr when the experiment was operating, as monitored using an ion gauge. The electron beam current was typically ~ 200 nA during the experiments, allowing the coincidence signal to be resolved from the background. The spectrometer operated under computer control, with the analyser tuning being optimised each time they were moved to a new angle. In this way any changes in the operating conditions as the experiments proceeded were minimised. A description of the computer control and optimisation systems used in these experiments can be found in [18].

For the experiments in section 5 a set of coincidence data was taken firstly with analyser 1 fixed in angle as in figure 1, while analyser 2 swept around the plane. Analyser 2 was then

set to the same fixed azimuthal angle, and analyser 1 then swept around the plane. At a given incident energy the coincidence measurements were accumulated for 3000 s at each angle, and up to 190 individual measurements were produced for a given molecular state. The accumulated data were then averaged for each angle, and the statistical error in the distribution of measurements used to assign an uncertainty.

The incident electron energy was calibrated against the 19.337 eV elastic resonance in helium [21], and the scattered and ejected electron energies were determined from inelastic scattering from this target. Helium was chosen for this purpose, as the inelastic spectrum is well known and can be clearly resolved.

Measurements presented in section 4 at the highest energy used here (100 eV above the IP for the $3\sigma_g$ state) were taken with each analyser selecting electrons with energy of 50 eV. For this set of data, the analysers were at the same azimuthal angle ($\theta_1 = \theta_2$). For the measurements in section 5, the analysers were adjusted to detect electrons with $(E_1, E_2) = (10 \text{ eV}, 10 \text{ eV})$ and with $(E_1, E_2) = (20 \text{ eV}, 20 \text{ eV})$. The incident electron beam was then scanned in energy to measure a binding energy coincidence spectrum, with the analysers fixed at $\theta_1 = \theta_2 = 45^\circ$. The binding energy spectra then allowed the relative strengths of the signals from each state to be ascertained, so that the data could be inter-normalised. Cross section measurements were then carried out by adjusting the incident electron beam energy to select either the $3\sigma_g$ or $1\pi_u$ state. Three data sets were accumulated for each state, by setting $\theta_1^{\text{Fixed}}(\theta_2^{\text{Fixed}}) = 45^\circ, 90^\circ$ and 125° . Since each set of data contained a common point, this allowed all data at a given energy to be inter-normalised. The experiments did not measure absolute cross sections, and so the data was then scaled to the molecular 3-body distorted wave (M3DW) calculations as described below.

3. Theory

A description of the theory was presented in [17] with more detail in [5], so it will not be repeated here. Results are presented for three different distorted wave models—the standard first order distorted wave Born approximation (DWBA), the M3DW approximation and the M3DW with the Ward–Macek (WM) approximation for PCI [22].

The important similarities and differences between these approximations are the following. All three models contain the interaction between the incoming electron and neutral target represented as a spherically symmetric initial state distorting potential. This potential is neutral asymptotically and is a screened nuclear potential for short range. In the spherical approximation, all target nuclei are spread over a thin spherical shell centred on the centre-of-mass. For N_2 , this means we place a charge of +14 on a thin shell with a radius of $1.0371 a_0$. For the electronic contribution, we calculate all the molecular wavefunctions using density function theory with a B3LYP/TZ2P basis set on a 3-dimensional numerical grid [5], use these wavefunctions to calculate the electronic charge density on this grid, and then use this density to

calculate the spherically symmetric electronic contribution. The final state distorting potential is calculated the same way, except the ionised electron is removed from the charge density such that this potential is asymptotically an ion. The Furness–McCarthy approximation [23] is used to calculate the effect of exchange between the continuum and bound electrons, and the Perdew and Zunger polarisation-correlation approximation [24] is used to determine this effect. Both the direct and exchange T-matrices are evaluated for all three approximations.

Finally, we use the orientation averaged molecular orbital approximation to calculate averaging over all molecular orientations [25]. Depending on the symmetry of the state being ionized, this average can be very small or even zero. For states like this, we average over the absolute value of the wavefunction instead of the wavefunction itself. If this average has multiple lobes, we make the first lobe positive, second lobe negative and so forth. For the $3\sigma_g$ state, we tried both types of averages and the shapes of the resulting cross sections were almost exactly the same, although there was a small magnitude difference. The presented results are for the average over the wavefunction. For the $1\pi_u$ state, we averaged over the absolute value of the wavefunction.

The main difference between the three calculations is the treatment of PCI—the final state PCI between the two electrons that is very important for collisions of this type. In the DWBA, PCI is included only to first order. In the M3DW, PCI is included exactly to all orders of perturbation theory, and in WM, the WM approximation is used to approximate PCI. There are two reasons to examine this approximation. First, since it is simply a factor times the DWBA amplitude, it is an easy way to include PCI in a standard DWBA calculation. Second, in some of our early work on molecules, it appeared that the exact PCI overestimated the effects of PCI and the WM approximation gave somewhat better agreement with experiment. In the comparison with experiment below, we show all three approximations that are calculated.

4. Coplanar doubly-symmetric experiments 100 eV above the $3\sigma_g$ IP

Following from the low energy results detailed in previous work [17], experiments were carried out at higher energies in both a coplanar doubly-symmetric geometry and with the electron gun set to 45° to the detection plane. The motivation for this work was to establish if the comparison between theory and experiment improved as the incident electron energy was increased.

Figure 2 shows the results of these studies plotted on a logarithmic scale for ionisation from the $3\sigma_g$ state. The incident electron energy was set to be 100 eV above the IP for this state, and the analysers were selected to have equal energy and equal azimuthal angles throughout data collection ($E_1 = E_2 = 50$ eV; $\theta_1 = \theta_2 = \theta$). The electron gun was positioned both in the scattering plane (coplanar geometry)

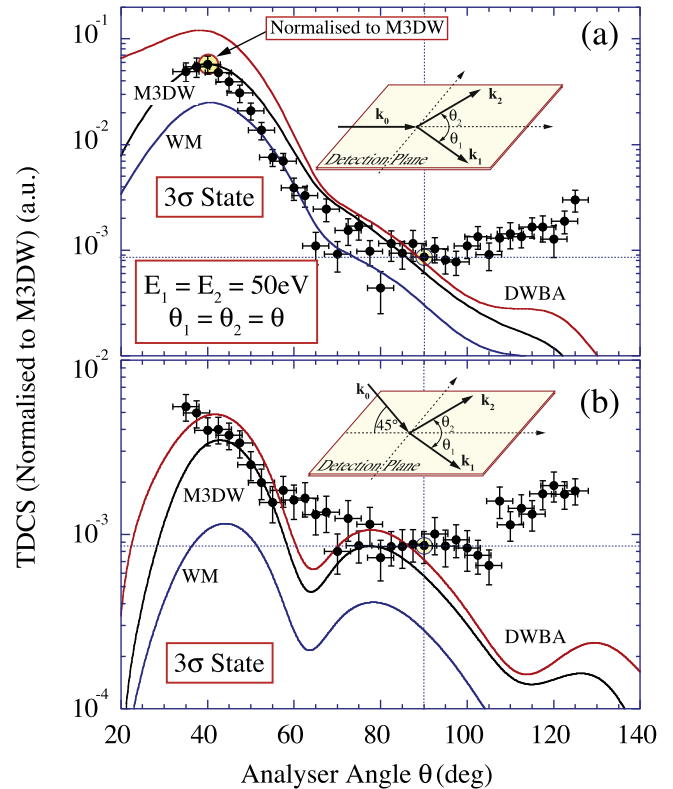


Figure 2. Measurements with incident electron energy 100 eV above the IP for the $3\sigma_g$ state, in both (a) a coplanar doubly-symmetric geometry and (b) for the incident electron beam direction \mathbf{k}_0 at an angle of 45° to the detection plane spanned by \mathbf{k}_1 and \mathbf{k}_2 . A common normalisation point exists between measurements when $\theta_1 = \theta_2 = 90^\circ$. DWBA, M3DW and WM theories are shown which have been convoluted with the experimental angular resolution. The data are normalised to the M3DW calculation at the forward peak in a coplanar geometry, so that a comparison can be made between theory and experiment.

and at an angle of 45° to the detection plane as shown in the inset figure. The data were normalised to the M3DW calculation at the forward peak in a coplanar geometry, since the experiments did not measure absolute cross sections. This is the same normalisation technique as was used previously [17], and allows a relative comparison to be made between the data and the different models.

The results from the series of experiments in [17] and as described here show that the ionisation cross section is sensitive to both the state from which ionisation occurs, and the collisional energy of the interaction. Comparison of the coplanar data at 100 eV above the IP for the $3\sigma_g$ state (figure 2(a)) shows considerably better agreement with theory than was found at lower energies [17], in particular for forward scattering where the M3DW calculation passes closely through the normalised data. In the backscatter direction beyond $\theta = 90^\circ$ however, the calculations predict that the magnitude of the cross section should continue to decrease, in contrast to what is observed.

When the electron gun is raised out of the detection plane (figure 2(b)), the cross section is seen to decrease as the scattering angle increases from 35° , and shows a plateau region from around 75° to 110° (although the uncertainties

and variations in the data are relatively large in this region). The data in figure 2(b) have been normalised to the coplanar data through the common point $\theta_1 = \theta_2 = 90^\circ$, which is depicted by the dotted lines and as circles in figure 2. The cross section is found to increase in the backscatter direction beyond 110° up to 125° . Further measurements were not possible beyond this angle due to the proximity of the analysers to each other. Since the TDCS must be zero at both 0° and 180° under these doubly-symmetric conditions, the results hence show evidence of two distinct peaks and a plateau region, with maxima around 35° , 90° and 125° .

The calculations all predict three peaks in the TDCS, with local minima that are much deeper than observed. The predicted forward minimum occurs at $\sim 60^\circ$, compared to the start of the plateau region at $\sim 75^\circ$ in the data. In the backscatter direction the calculated minimum occurs around 110° , in closer agreement with measurement. All calculations underestimate the cross section in the backscattering region, whereas in the forward direction the DWBA model appears to yield the overall best fit to the data. Since electron backscattering requires a strong interaction between the target nuclei and the scattered electrons, the backscatter results imply that the models are underestimating the magnitude of the nuclear force in the interaction. This is probably due to the spherical averaging process that spreads the nuclear charge over a thin spherical shell.

5. Coplanar measurements with fixed angles

To further test theory, asymmetric coplanar measurements were conducted with one of the electrons detected at a fixed angle, as in figure 1. Prior to measurement of the cross sections, the energy of the detected electrons was set to either 10 or 20 eV, and the energy of the incident electron was adjusted in steps of 0.125 eV to obtain a binding energy spectrum from the coincidence signals. These experiments were carried out with $\theta_1 = \theta_2 = 45^\circ$, as this produced a strong signal above the background. The incident energy hence passed through ionisation from both the $3\sigma_g$ and $1\pi_u$ states. This allowed the ratio of the coincidence rates to be determined from each state, by fitting a Gaussian to the resolved peaks. Figure 3 shows an example of a binding energy spectra obtained for outgoing electrons with energy of 10 eV. By taking several spectra, the ratio of cross sections from these states was determined to be $(1\pi_u^{45^\circ} : 3\sigma_g^{45^\circ})^{10/10\text{eV}} = (49\% \pm 6\%)$. Similar measurements at 20 eV outgoing energy found this ratio to be $(1\pi_u^{45^\circ} : 3\sigma_g^{45^\circ})^{20/20\text{eV}} = (23\% \pm 3\%)$. These ratios were then used in the inter-normalisation procedure discussed below.

5.1. Measurements for outgoing electron energies of 10 eV

Figure 4 shows the results for outgoing electron energies of 10 eV, at three fixed angles of 45° , 90° and 125° for both $3\sigma_g$ and $1\pi_u$ states. The data are placed on a logarithmic scale to allow comparison to the different models, which have all been

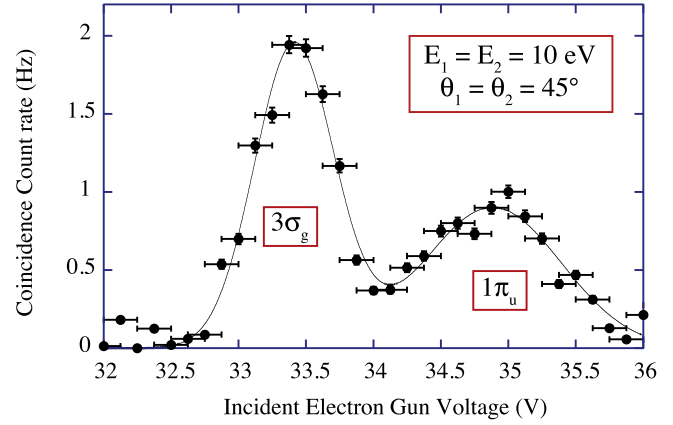


Figure 3. Example of a binding energy spectrum, taken for outgoing electron energies of 10 eV at scattering angles of 45° . The individual $3\sigma_g$ and $1\pi_u$ states are well resolved, allowing the relative ratios of the TDCS from each state to be determined.

convoluted with the angular resolution of the experimental apparatus.

Since the experiments do not measure absolute cross sections, the data are again normalised to the maximum of the M3DW calculation for the $3\sigma_g$ state, as was carried out in [17]. This normalisation point is shown in figure 4(a). The data for the $3\sigma_g$ state in figures 4(a)–(c) were then inter-normalised through their common points, allowing for reflection symmetry in the detection plane as described by figure 1. These points are shown in the figure. As an example, in figure 4(b) the left-hand point shows where $\text{TDCS}(\theta_1 = 45^\circ, \theta_2 = 90^\circ) \equiv \text{TDCS}(\theta_1 = 90^\circ, \theta_2 = 45^\circ)$, whereas the right-hand point shows where $\text{TDCS}(\theta_1 = 125^\circ, \theta_2 = 90^\circ) \equiv \text{TDCS}(\theta_1 = 90^\circ, \theta_2 = 125^\circ)$.

Figures 4(d)–(f) show results for the $1\pi_u$ state, inter-normalised to the $3\sigma_g$ state through the ratio determined from the binding energy spectra (as in figure 3). The axes for this set of data are adjusted to be the same as for the $3\sigma_g$ state, allowing direct comparison of the results. The relative common points are also shown for this state. The inter-normalisation procedure hence allows all six data sets to be re-scaled to the M3DW calculation, as set in figure 4(a).

The results in figure 4 show that none of the calculations adequately describe the data at this energy. For the $3\sigma_g$ state at a fixed angle of 45° , all calculations predict minima around 45° in contrast to measurement, and predict maxima around 80° whereas the data finds a minimum in this region. Calculations for the $1\pi_u$ state at this angle (figure 4(d)) are slightly better as their magnitudes are closer to experiment, however once again the predicted structures do not emulate the data. For a fixed angle of 90° , all calculations predict a broad minimum at $\sim 90^\circ$ for both states. The experiments find a shallow minimum at $\sim 100^\circ$ for the $3\sigma_g$ state and at $\sim 90^\circ$ for the $1\pi_u$ state. The calculations are hence in better agreement here, however for the $3\sigma_g$ state the calculations are broadly an order of magnitude larger than the normalised data. For a fixed scattering angle of 125° , there is little agreement between the calculations and the data for either

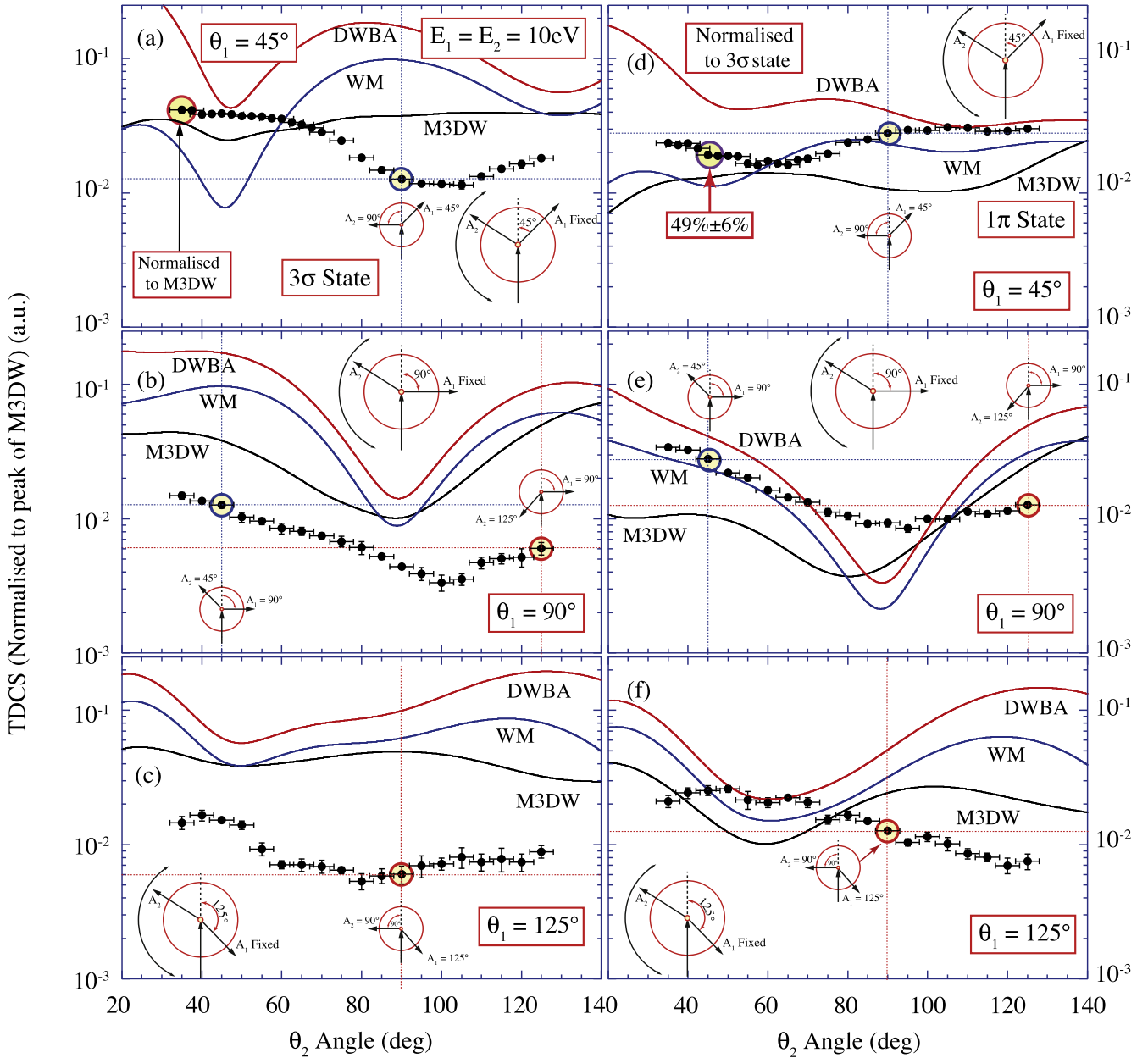


Figure 4. Results for outgoing energies of 10 eV, for the $3\sigma_g$ state (a)–(c) and the $1\pi_u$ state (d)–(f). The data are normalised to the peak of the M3DW calculations in (a) as described in [17], since the experiments do not measure absolute cross sections. All other data are then inter-normalised at the angles shown, as described in the text. All calculations are convoluted with the angular resolution of the apparatus.

state, and once again the predicted cross section for the $3\sigma_g$ state is much larger than measured. The models clearly fail to fully include the correct physics of the interaction at these energies, as was also found in [17].

5.2. Results for outgoing electron energies of 20 eV

Figure 5 shows the results at outgoing energies of 20 eV, again for fixed angles of 45° , 90° and 125° . The data are once more placed on a logarithmic axis to allow comparison with figure 4, and are set to the same scale for both data sets.

The data in figure 5 are again normalised to each other and to the peak of the M3DW calculations, by consideration

of the binding energy spectra at this energy. The common points between data sets are once more shown.

The agreement between experiment and theory improves under these kinematic conditions, however significant differences remain. At a fixed scattering angle of 45° all calculations are closer in magnitude to the data for both states. In this case the M3DW and WM calculations are closer than the DWBA calculation, indicating that PCI are playing a significant role here. All calculations again predict broad minima in the forward direction for the $3\sigma_g$ state in contrast to measurement, and predict maxima around 70° which disagrees with observations. For the $1\pi_u$ state (figure 5(d)), both WM and M3DW calculations align reasonably well with the measurements.

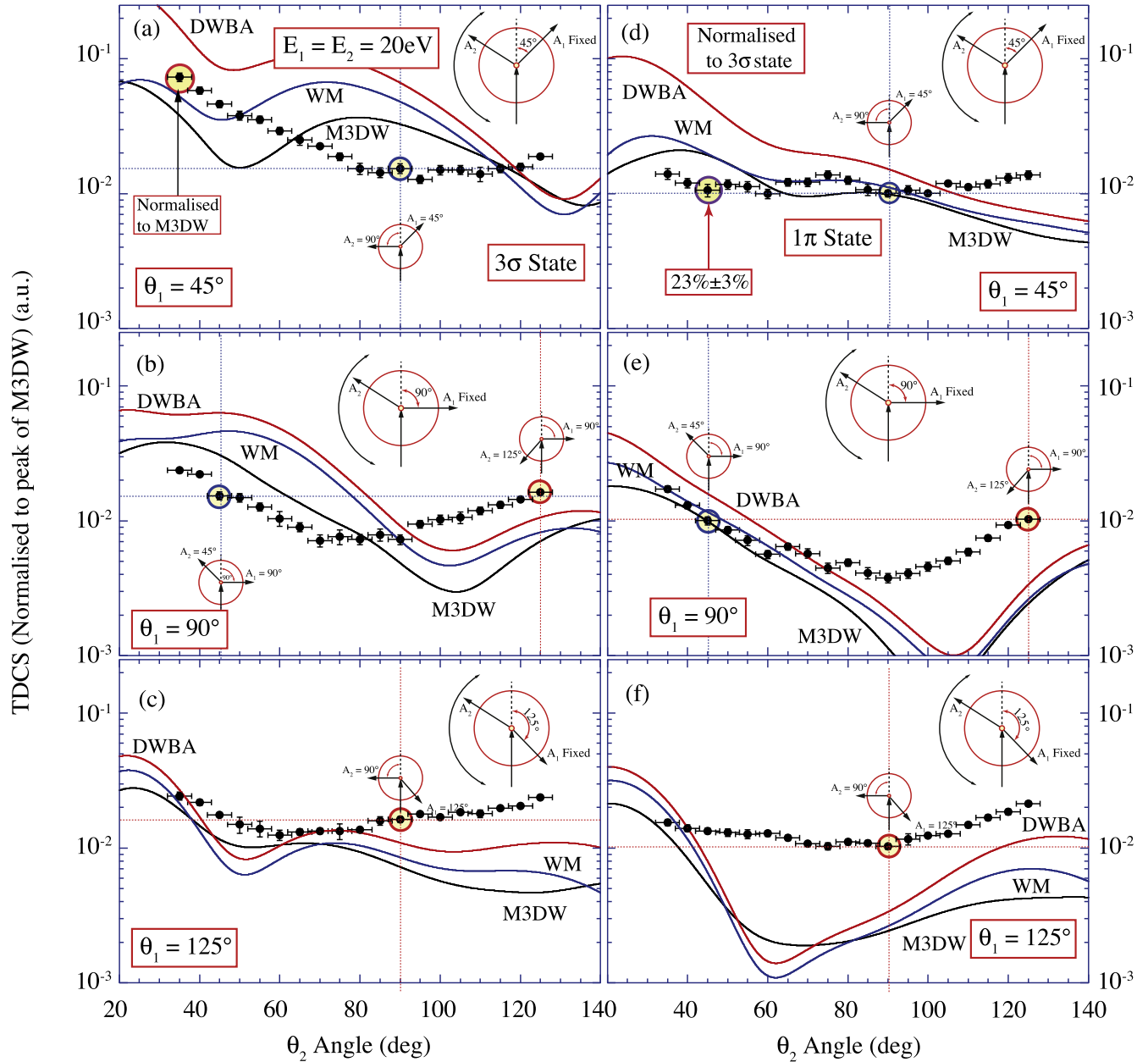


Figure 5. Results for outgoing electron energies of 20 eV for the $3\sigma_g$ and $1\pi_u$ states. The data are normalised to the peak of the M3DW theoretical calculations in (a). All other data are then inter-normalised at the angles shown, as described in the text. All calculations are convoluted with the angular resolution of the apparatus.

At a fixed angle of 90° for the $3\sigma_g$ state (figure 5(b)), the M3DW calculation yields the closest fit to the data, however this calculation predicts a minimum at $\sim 105^\circ$ whereas the experiment finds a minimum at $\sim 70^\circ$. By contrast, all three calculations for the $1\pi_u$ state are in closer agreement with the data for forward scattering (figure 5(e)). The models again predict minima at around 105° , whereas the data finds a local minimum at 90° .

For a fixed angle of 125° all theories predict a cross section that is reasonably close to measurements for the $3\sigma_g$ state (figure 5(c)), whereas all fail to emulate the data for the $1\pi_u$ state (figure 5(f)). For the $1\pi_u$ state the predicted cross sections in the forward direction all have deep minima at around 65° , which is not reproduced in the data.

The wide variation found here when comparing theory to experiment makes it difficult to ascertain where improvements can be made to the models. It appears that the calculations from the $1\pi_u$ state overall are in better agreement with the data than for the $3\sigma_g$ state, and so it may be that the $1\pi_u$ target wavefunction used here is better than for the $3\sigma_g$ state. The magnitudes and shapes of the predicted cross sections for all models are however mostly in poor agreement with experiment, and indeed do not follow any particular trend as the fixed scattering angle increases. The calculations do appear to improve as the energy is increased, which is consistent with findings from other studies [17]. This is perhaps to be expected for these types of calculations, which have proven to be successful particularly at higher energies.

6. Discussion and conclusions

The results from experiments and calculations detailed here show that the ionisation cross section is sensitive to both the state from which the ionisation occurs, and the collisional energy of the interaction. Comparison of coplanar experimental data at 100 eV above the IP for the $3\sigma_g$ state shows better agreement with theory than found in previous work [17], in particular for forward scattering where the M3DW calculation passes closely through the data. In the backscatter direction however, the calculations predict that the magnitude of the cross section should decrease, in contrast to observation. When the electron gun is raised out of the detection plane the calculations again agree with the data in the forward direction, however they all predict a deep minimum at $\sim 60^\circ$ which is not observed. Once again in the backscattering direction the calculations fail to agree with measurement.

The comparison between theory and experiment at energies 20 and 40 eV above the IP of the $3\sigma_g$ and $1\pi_u$ states is much less satisfactory. Six inter-normalised sets of data were obtained at each energy, allowing a rigorous test of calculation over a range of kinematics. Under certain conditions the calculations emulated the data reasonably well, however, in general, the magnitude and shape of the predicted cross sections fail to agree with the data. No definitive conclusions can be drawn from these results, however it does appear that the calculations for the $1\pi_u$ state more closely agree with experiment, and that the model improves as the energy is increased.

One possible reason for the poor agreement between theory and experiment found here might be due to the averaging of molecular orbitals approximation that was adopted, as discussed in section 3. Attempts were made in this work to calculate the cross sections using a ‘proper averaging’ approach (i.e. by calculating the TDCS for each orientation of the molecule, then averaging the final results), however these calculations would not converge. Clearly more work is required to ascertain where improvements can be made to the models, so that they can more realistically predict the data.

Acknowledgements

AS would like to thank the University of Manchester for financial support through their overseas student award. AM and MH would also like to thank the EPSRC for funding this project under award R120272. SA and DM acknowledge the support of the US National Science Foundation under grant no. PHY-1505819 and CN would like to acknowledge the support of the National Natural Science Foundation of China under grant no. 11174175.

ORCID iDs

Andrew James Murray  <https://orcid.org/0000-0001-9546-6644>

References

- [1] Barklem P S, Osorio Y, Fursa D V, Bray I, Zatsarinny O, Bartschat K and Jerkstrand A 2017 *Astron. Astrophys.* **606** A11 and references therein
- [2] see e.g. Rauch T, Quinet P, Knörzer M, Hoyer D, Werner K, Kruk J W and Demleitner M 2017 *Astron. Astrophys.* **606** A105
- [3] Griffin D C, Pindzola M S, Shaw J A, Badnell N R, O’Mullane M and Summers H P 1997 *J. Phys. B: At. Mol. Opt. Phys.* **30** 3543
- [4] Bug M U, Baek W Y, Rabus H, Villagrasa C, Meylan S and Rosenfeld A B 2017 *Radiat. Phys. Chem.* **130** 459
- [5] Madison D H and Al-Hagan O 2010 *J. At. Mol. Opt. Phys.* **2010** 367180
- [6] Colgan J, Al-Hagen O, Madison D H, Kaiser C, Murray A J and Pindzola M S 2009 *Phys. Rev. A* **79** 052704
- [7] Avaldi L, Camilloni R, Fainelli E and Stefani G 1992 *J. Phys. B: At. Mol. Opt. Phys.* **25** 3551
- [8] Gao J, Madison D H and Peacher J L 2005 *Phys. Rev. A* **72** 032721
- [9] Murray A J, Hussey M J, Gao J and Madison D H 2006 *J. Phys. B: At. Mol. Opt. Phys.* **39** 3945
- [10] Naja A, Staicu-Casagrande E M, Lahmam-Bennani A, Nekkab M, Mezdari F, Joulakian B, Chuluunbaatar O and Madison D H 2007 *J. Phys. B: At. Mol. Opt. Phys.* **40** 3775
- [11] Murray A J, Hussey M J, Kaiser C, Gao J and Madison D H 2007 *J. Electron Spectrosc. Relat. Phenom.* **161** 11
- [12] Lahmam-Bennani A, Staicu-Casagrande E M and Naja A 2009 *J. Phys. B: At. Mol. Opt. Phys.* **42** 235205
- [13] Toth I and Nagy L 2011 *J. Phys. B: At. Mol. Opt. Phys.* **44** 195205
- [14] Murray A J 2015 *J. Phys. B: At. Mol. Opt. Phys.* **48** 245203
- [15] Brauner M, Briggs J S and Klar H 1989 *J. Phys. B: At. Mol. Opt. Phys.* **22** 2265
- [16] Read F H 1985 *Electron Impact Ionization* ed T D Mark and G H Dunn (Vienna: Springer) p 42
- [17] Sakaamini A, Amami S, Murray A J, Ning C and Madison D 2016 *J. Phys. B: At. Mol. Opt. Phys.* **49** 195202
- [18] Murray A J, Turton B C H and Read F H 1992 *Rev. Sci. Instrum.* **63** 3346
- [19] Murray A J, Read F H and Bowring N J 1997 *J. Phys. B: At. Mol. Opt. Phys.* **30** 387
- [20] Hussey M J and Murray A J 2005 *J. Phys. B: At. Mol. Opt. Phys.* **38** 2965
- [21] Brunt J N H, King G C and Read F H 1977 *J. Phys. B: At. Mol. Phys.* **10** 1289
- [22] Ward S J and Macek J H 1994 *Phys. Rev. A* **49** 1049
- [23] Furness J B and McCarthy I E 1973 *J. Phys. B: At. Mol. Phys.* **6** 2280
- [24] Perdew J P and Zunger A 1981 *Phys. Rev. B* **23** 5048
- [25] Gao J, Peacher J L and Madison D H 2005 *J. Chem. Phys.* **123** 204302